Preparation and co-dispersion of TiO_2-Y_2O_3 suspensions through the study of their rheological and electrokinetic properties

F. La Lumia, L. Ramond, C. Pagnoux, G. Bernard-Granger

Preparation and co-dispersion of TiO_2-Y_2O_3 suspensions through the study of their rheological and electrokinetic properties

F. La Lumia [a], L. Ramond [a], C. Pagnoux [b], G. Bernard-Granger [a]

[a] CEA, Nuclear Energy Division, Research Department on Mining and Fuel Recycling Processes, SFMA, BP 17171, F-30207 Bagnols sur Cèze, France

[b] Institute of Research for Ceramics (IRCER), 12 rue Atlantis, F-87068 Limoges, France

Abstract

The development of Generation IV sodium-cooled fast reactors (SFR) is currently studied by several countries. These new type of reactors are intended to use new types of UO_2-PuO_2 nuclear fuels. In order to produce them, new innovative liquid routes are investigated. Among these liquid route processes, some involve at first the preparation of high solid content water-based suspensions. This key step needs to be investigated in order to obtain highly and easily processable suspensions, featuring optimal viscosity and dispersion state. The structures and properties for all intermediate and final products involved in such ceramic manufacturing processes are heavily affected by these suspension characteristics. Therefore, they are critical to ensure a compliant final product (i.e. fuel pellets) with the required density, homogeneity, mechanical strength and absence of defects. In this scope, preparation process of such suspensions was developed by the use of UO_2 and PuO_2 surrogating (i.e. mimicking) powders, TiO_2 and Y_2O_3 respectively.

1. Introduction / Objectives

The current manufacturing of UO_2-PuO_2 MOX fuel pellets is carried out by a dry route process [1], through steps involving fine powders (grinding, mixing and pressing). In order to limit dust retention in glove boxes and thus to decrease workers dose rates, new liquid routes are investigated. These new processes are also expected to grant a pellet microstructure containing less defects (cracks, voids) as well as a more homogenous U-Pu distribution in the final pellets compared to the dry process.

The key step of these liquid route processes is the preparation of a stable and well-dispersed aqueous powder suspension [2] (in the present case UO_2 and PuO_2 powders), in order to have a charged, yet fluid and settling-resistant suspension. From these suspensions, two liquid routes for pellet shaping are considered. The first one is the spray-freeze drying [3] of the suspension followed by a granules pressing step and the second one consists in slip casting the suspension into porous molds [4]. The research work presented in this paper is focused on the preparation of the powder suspensions, mainly through the study of their rheological and electrokinetic (i. e. particle surface charge) properties [5, 6, 7]. Indeed, these suspension characteristics have a deep influence on the structures and properties of all intermediate products (granulated powders and green pellets) and final products (sintered pellets) involved in such ceramic manufacturing processes [8-11].

In the colloidal processing of ceramic powders, it is essential that the powder particles are completely dispersed so that neither agglomerates nor aggregates form [12]. It is these aggregates that give rise to flaws in the final sintered product, causing reductions in strength and reliability [13]. These aggregates form in submicron powders due to the attractive Van der Waals forces. Traditionally, in colloidal processing those attractive forces can be countered by a greater repulsive force separating the particles from one another. This can be achieved in two ways: either i) by the addition of electric charges at the particles surface so that they repel one another - termed electrostatic stabilization -, ii) by the addition of a polymeric molecule, which when adsorbed onto the powder surface prevents the particles from physically coming close enough for the attractive force to cause flocculation; this is termed steric stabilization. A combination of these two effects is termed electrosteric stabilization and is the probable stabilization mechanism when polyelectrolytes are adsorbed onto the particles [14].

It is essential to know how much dispersant to add to each system for process optimization purposes (suspension flowability and green product debinding step) as well as to avoid problems associated with unadsorbed dispersant in the suspension, i.e. compression of the double layer as a polyelectrolyte acts as just like an electrolyte.

For easier handling and processing during the investigation, experiments were made with surrogate powders, i.e. non-radioactive powders which have some physicochemical properties similar to those of the radioactive powders UO_2 and PuO_2. To select each surrogating powder, properties considered are the ones which are relevant of the investigated process or application. In the present case, both considered processes (spray-freeze-drying and slip casting) imply powders suspended in aqueous media at high concentrations. Thus, the UO_2 and PuO_2 powders properties to mimic are the following:

- the size and morphology of the powder particles, which are related to the suspension rheology,
- the Point of Zero Charge (PZC) of the materials, which are related to the electrokinetic properties of the particles in suspension (i. e. particle surface charge).

Thus, according to these criteria, the surrogating powders chosen for this study were TiO_2 and Y_2O_3, selected for their suspension properties (Point of Zero Charge and particle morphology) to surrogate UO_2 and PuO_2, respectively.

The aim of the research reported in this paper is to determine how to prepare, from the raw TiO_2 and Y_2O_3 powders and some organic additives, aqueous TiO_2-Y_2O_3 suspensions that have the appropriate features and characteristics for spray-freeze drying or slip casting processes. The suspension desired features are the following:

- a solid content high enough to grant a fast water removal in order to form the green product fast and with an optimal porosity,
- a viscosity low enough to allow pumping, spraying or slip-casting of the suspension,
- settling resistance (stability) and dispersion to prevent suspension powders sedimentation and thus grant physical and chemical homogeneity of the suspension as well as of the subsequent green and final products.

The surrogate powders TiO_2 and Y_2O_3 were studied both separately and mixed together in proportions of 15 at% Y (Y/(Y+Ti)). Such proportions were chosen to represent a trade-off between the atomic percent of Pu in the light water reactor MOX fuels (3-10 at% Pu) and in the fuels envisaged for Generation IV fast neutron reactors (20-30 at% Pu).

2. Experimental section

2.1 Analytical devices and techniques

2.1.1 Raw powders characterization devices

Four main features of the raw powders were characterized:

- Specific surface areas were assessed with BET (Bruauer, Emett, Teller) N_2 sorption method with a Micromeritics ASAP 2020 surface area analyzer.
- Densities were measured with a Micromeritics AccuPyc 1340 helium pycnometer.
- Particle morphologies were determined using a Cambridge Instruments Stereoscan S 260 Scanning Electron Microscope (SEM).
- Particle size distributions were measured with a Horiba LA-950 liquid granulometer. In order to prevent particle agglomeration during measurements, suspensions were ultrasonicated for 30 s prior to the measurements. Moreover, 0.5 wt% (based on dry powder weight) of Darvan CN dispersant was added to the Y_2O_3 powder, given its low surface charge in suspension (see Fig. 2). TiO_2 powder granulometry was measured without any dispersant given its rather high negative surface charge (see Fig. 3).

2.1.2 Rheometer

A Rheolab QC rheometer (Anton Paar) equipped with a CC27 cylindrical geometry and thermostated at 20°C, was used to assess suspension viscosity. Prior to the measurements, a constant shear rate of 1500 s^{-1} was applied for 120 s to bring each sample to the same rheological past and thus grant measurement reproducibility. Rheology measurements were conducted with a ramp of shear rate from 1 to 1500 s^{-1} imposed to the sample, with 30 s delay between each point to let time for steady state to establish. Each experiment of shear rate ramp lasted 10 min, for a total of 20 points acquired per experiment.

Concentrated suspensions for rheological measurements were prepared with various solid contents in the range 25–40 %v. by mixing water with dispersant in a flask and then raw powders were added under mechanical stirring. Eventually, enough yttria-stabilized zirconia grinding balls (diameters 3/10/15 mm in volume proportions of 70/10/20) were added to outcrop at the suspension surface. Hereafter, the suspension was let to roll for 20 hrs on a roller mixer (RM-5, CAT) at 15 rpm. This process is known in literature to yield low viscosity suspensions [15, 16]. Finally, suspension was degassed with a Thinky ARE-250 (Intertronics) planetary mixing and degassing machine for 3 min at 1100 rpm to remove air bubbles entrapped in the suspension.

2.1.3 Acoustophorometer

Zeta potential measurements were conducted as a function of the pH on the raw materials dispersed at 1.25 %v. in deionized water with an ESA analyser (AcoustoSizer II S flow through system, Colloidal Dynamics). The apparatus includes sensors for measuring pH, ionic conductivity, and temperature. The zeta potential was obtained from the ESA voltage data treated with the AcoustoSizer II operation software by using the Smoluchowski relationship. This relationship is relevant when the thickness of the electrical double layer is small compared to the particle radius [5, 17]. Experimental data proved this hypothesis to be verified in the present work. Zeta potential measurements at different pH were made with the automated AcoustoSizer II pH titration system using 1.0 mol/L sodium hydroxide or 1.0 mol/L hydrochloric acid solutions. The starting pH was the natural pH of the suspension (represented by hollow dots on titration curves) before any acid or base addition. pH titrations were made starting from the suspension natural pH to acid or basic pH by adding either hydrochloric acid or sodium hydroxide, respectively. All zeta potential measurements were performed with 10^{-2} mol/L sodium chloride as background

electrolyte to keep the ionic strength constant through the whole investigated pH range (3-12). However, pH titrations implying Y_2O_3 powder were restricted to pH range 7-12 due to Y_2O_3 dissolution occurring below pH 6 [18, 19].
All suspensions for acoustophorometric measurements were prepared with 1.25 %v solid content. First, distilled water and dispersant (if any) were mixed under magnetic stirring for 60 s, then oxide powders were added while stirring for further 5 min. Hereafter the suspension was ultrasonicated with an ultrasonic probe (Vibra-cell 75041, BioBlock Scientific) for 2 min to break particle agglomerates. Finally, the suspension was let for 15 min on a roller mixer (CAT, RM-5, Germany) operating at 15 rpm.

2.1.4 Sedimentation tests

Sedimentation experiments were conducted for pure TiO_2 and Y_2O_3 diluted suspensions and mixed TiO_2-Y_2O_3 diluted suspensions.
The diluted suspensions were prepared following the protocol presented in part 2.1.3. Immediately after preparation, the suspensions were allowed to settle in closed tubes for a total of 28 days. In such conditions, a clear supernatant was observed and the height of sediment was measured accurately as a function of time.

2.2 Raw chemicals

Darvan CN (Vanderbilt Minerals LLC) was used as a dispersant, in the form of a ready-to-use 25 wt% aqueous solution. This polymer is an ammonium polymethyl methacrylate with an average molar weight of 15,000 g/mol.
Dispersant concentration will be expressed in wt% of the dry powder present in the considered suspension.
Sodium hydroxide and hydrochloric acid were purchased from Sigma-Aldrich in the form of 1.0 mol/L solutions and used as-received.

3. Results and discussion

3.1 Raw powders characteristics

The main features of the surrogate and active powders are compared and summarized in Table 1.

3.1.1 TiO_2 powder characteristics

Custom-made titanium dioxide (Marion Technologies, anatase form, purity 99.9 %) has an average particle size of 100 nm. Size distribution of the TiO_2 powder (Fig. 1) shows a bimodal distribution with two populations at 70 nm and 0.8 µm. A specific surface area of 12 m^2/g and a powder density of 3.78 g/mL were assessed. The TiO_2 particles are aggregates made of nanometer-sized spheres (depicted in Table 1).

3.1.2 Y_2O_3 powder characteristics

Yttrium oxide powder (“Grade C” powder, purity 99.95%) was purchased from H.C. Starck. Y_2O_3 powder showed an average particle size of 1.8 µm and a bimodal size distribution (Fig. 1) with populations at 250 nm and 1-7 µm. Moreover, a specific surface area of 14 m^2/g and a density of 5.01 g/mL were measured for the Y_2O_3 powder. Its particle morphology (depicted in Table 1) was proven to be plate-shaped.

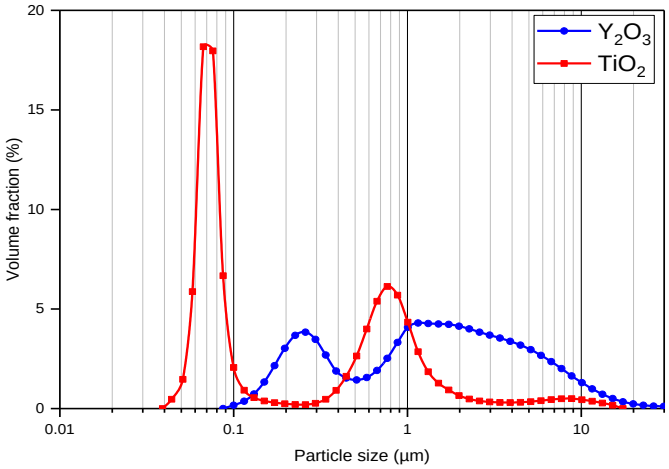

Fig. 1: Size distribution obtained by liquid granulometry of the Y_2O_3 (with 0.5 wt% Darvan CN dispersant) and TiO_2 (without dispersant) powders.

As one can see in Table 1, the TiO_2 and Y_2O_3 surrogate powders have most of their suspension-relevant characteristics (i. e. PZC, particle morphology and size distribution) close to the radioactive powders UO_2 and PuO_2, respectively. However, the surrogate powders densities are 2 to 3 times lower than the active powders densities. The powder density obviously plays an important role in particle settling rate (and thus suspension stability) when suspended in liquid media. Indeed, UO_2 and PuO_2 powders are very dense and it was practically impossible to find commercial surrogate powders with such high densities, while having their other main suspension-relevant properties (i. e. PZC, particle morphology and size distribution) close to the ones of the radioactive powders. Thus, TiO_2 and Y_2O_3 powders appeared to be the best trade-off between all the suspension-relevant characteristics of the radioactive powders to surrogate.

Powder formula	Supplier, reference	Purity (%)	Particle size (µm)	Particle morphology	Density ($g.cm^{-3}$)	Specific surface area ($m^2.g^{-1}$)	Expected point of zero charge (from litterature)	SEM micrography
UO_2 (dry route process)	N/A	N/A	0.1 + 0.8	Nanophere aggrgates	10.5	2	5.5 [20,57]	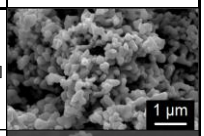
TiO_2	Marion Technologies	99.9	0.07 + 0.8		3.78	12	5.5 [12,20,21]	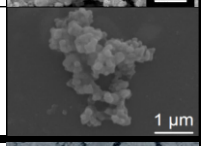
PuO_2	N/A	N/A	1 to 10	Platelets	11.0	6	9 [20]	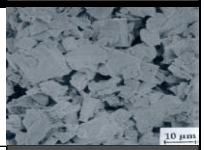
Y_2O_3	H.C.Starck, grade C	99.95	0.25 + 1 to 7		5.01	14	9 [19,20]	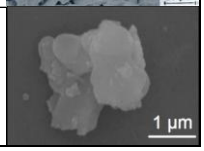

Table 1: Main characteristics of the active powders UO_2, PuO_2 and their respective surrogating powders TiO_2 and Y_2O_3.

3.2 Powder treatments

3.2.1 Y_2O_3 powder treatment

In diluted suspension (1.25 %v solid content), the raw Y_2O_3 powder displayed an unusual PZC value of 12 (Fig. 2) rather than the value of 9 encountered in the literature [19, 20]. Thus, a washing treatment was applied to the raw Y_2O_3 powder, aiming to modify its PZC. Powder washing was performed by suspending Y_2O_3 powder in distilled water at a solid concentration of 150 g/L and stirring the suspension for 18 hrs. Eventually, the suspension was centrifuged with a Thermo-Fisher IEC 40 centrifuge. The resulting cake was separated from the supernatant and dried at 120°C for 48 hrs to constant mass. The effects of the powder treatment on the Y_2O_3 diluted suspension (1.25 %v solid content) zeta potential are displayed in Fig. 2 and compared with the raw Y_2O_3 powder zeta potential. The washing process was able to decrease the Y_2O_3 PZC from 12 to 8.7. The suspension natural pH was also decreased from 10 to 7.5 by the washing process. All characteristics displayed in part 3.1.2 about the Y_2O_3 powder were not modified by the washing process.

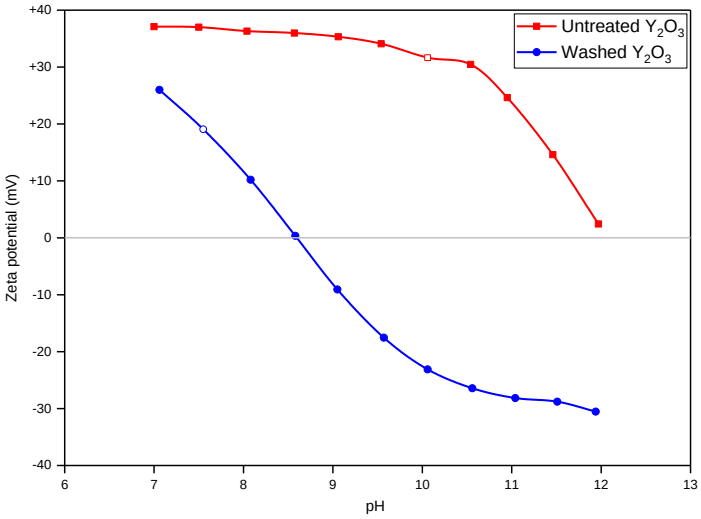

Fig. 2: Zeta potential of the as-received and washed Y_2O_3 powder vs. pH (hollow dots correspond to natural pH).

3.2.2 TiO_2 powder treatment

In diluted suspension (1.25 %v solid content), the raw TiO_2 powder retains a high negative surface charge on the whole pH range investigated (3-12) and does not exhibit any PZC on the pH range 3-12. This result is quite surprising because an average PZC of 5-6 is generally given in the literature for most of the TiO_2 powders of any crystalline form [12, 21, 20]. However, some authors highlighted that the TiO_2 PZC is very sensitive to the powder synthesis process and to the presence of impurities [22, 24, 28]. Thus, PZC of TiO_2 powders encountered in literature may vary widely [22, 23, 24]. Suttiponparnit *et al.* [22] have also proven that primary particle size has a strong influence on TiO_2 PZC; the PZC decreases when particle size increases, due to the change of the surface/volume ratio. A number of authors [25, 26, 27] even reported only negative electrokinetic potentials for TiO_2 powders. This would suggest the PZC of TiO_2 being positioned at very low pH values.
Washing or calcination treatments had only minor effects on the TiO_2 electrokinetic behavior, reducing its negative surface charge, but not enough to let a PZC appear. The surface charge reduction is believed to be caused by the removal of adsorbed species by the washing treatment, or the removal of surface hydroxyl groups in the case of the calcination treatments, as observed by Cornell *et al.* [28].
Taking these results into account, further experiments conducted in the scope of this paper were made with:

- the washed Y_2O_3 powder, to ensure for the Y_2O_3 surrogate powder a PZC of ~ 9 (close to the PZC of PuO_2),
- the as-received (raw) TiO_2 powder because washing or calcination had no effect on its PZC value.

3.3 Dispersion of pure TiO_2 or Y_2O_3 suspensions

Optimal contents of Darvan CN dispersant were assessed both by acoustophoresis (Fig. 3) and rheology experiments (Fig. 4) on pure TiO_2 or Y_2O_3 suspensions.

3.3.1 Pure suspensions electrokinetic properties

Darvan CN has almost no effect on TiO_2 particles surface charge, which remains below – 30 mV on the whole pH range 3-12, regardless the amount of Darvan CN added (Fig. 3). This is due to the already highly negative-charged particle surface, where adding more negative charges with polyelectrolyte adsorption hardly modify the particles zeta potential. Adding high amounts (1%) of Darvan CN even slightly worsens the suspension dispersion as the free (unadsorbed) polyelectrolyte induces a compression of the electrical double layer and thus decreases the zeta potential.

Addition of a small amount (0.1 %) of Darvan CN to the Y_2O_3 suspensions first shifted the positive zeta potential to slightly negative values as it adsorbs on the positive-charged particle surface (Fig. 3). Adding more Darvan CN (0.1 – 0.3 %) makes the zeta potential more negative. Further addition of dispersant increases the zeta potential further until a plateau region was reached where addition of more dispersant does not affect the zeta potential (0.3 – 0.5 %). Dispersant addition beyond this plateau (> 0.5 %) slightly decreases the zeta potential as particle surface is now saturated with adsorbed polymer. The increasing free (unadsorbed) polymer concentration causes compression of the particle electrical double layer and reduces the zeta potential. Hence, the minimum amount of dispersant required to stabilize the Y_2O_3 powder is about 0.3 wt% (in diluted media). However, the PZC of the Y_2O_3 suspension containing 0.5 wt% Darvan CN is lower (i. e. more shifted to lower pH values) than the one of the Y_2O_3 suspension containing 0.3 wt% Darvan CN, indicating that the former suspension is more dispersed than the latter. Thus, the best amount of Darvan CN to stabilize Y_2O_3 suspensions is stated to be 0.5 wt%. The highly negative plateau value of the obtained zeta potential (- 40 mV) gives an indication of the good suitability of the Darvan CN to stabilize the Y_2O_3 powder.

The presence of Darvan CN in suspensions tends to increase the pH from 6-7 (natural pH) to about 9-10. Acid-base properties of Darvan CN ionic groups (carboxylates and ammonium ions) act like a pH buffer, shifting the suspensions pH to values close to the NH_4^+/NH_3 pKa. At pH 9-10, all carboxylate groups are dissociated (the pKa of these groups is about 5 [29]), so the polymer chains are fully negatively charged.

Adsorption mechanisms of polyelectrolytes like Darvan CN and other polycarboxylates have already been extensively investigated in the literature, especially by Wisniewska and Chibowski [29, 30, 31]. It occurs mainly through hydrogen bonds between particle surface hydroxyl groups (-OH) and polymer carboxylate groups ($-CO_2H$ / $-CO_2^-$). These hydrogen bonds can be formed not only by non-dissociated polymer carboxylate groups, but also by dissociated ones, so that adsorption of polycarboxylates on the metal oxide surface undergoes even under the conditions of adsorbate–adsorbent repulsion [32]. At high pH ($pH > pH_{pzc}$), the polymer carboxylate groups are fully dissociated ($-CO_2^-$ form) and the particle surface is also negatively charged, which results in a highly negative overall surface charge. At low pH ($pH < pH_{pzc}$), the particle surface is positively charged and the polymer carboxylate groups are more or less negatively ionized, depending on the pH and carboxylate pKa (~ 5) relative values. So the overall particle charge is weakly positive or negative depending on the pH closeness to the carboxylate pKa.

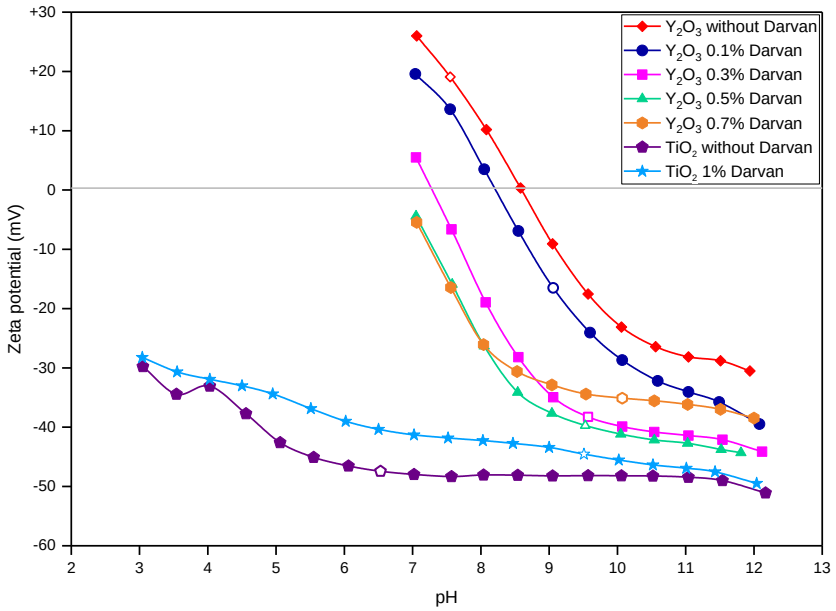

Fig. 3: Zeta potential of 1.25 %v TiO_2 and Y_2O_3 suspensions vs. pH at different Darvan CN concentrations (hollow dots correspond to natural pH).

3.3.2 Pure suspensions rheological properties

The rheological properties of TiO_2 and Y_2O_3 concentrated suspensions (25 and 30 %v respectively) displayed in Fig. 4 revealed that both suspensions exhibit a shear-thinning behavior, which is common for ceramic suspensions [33, 34, 35, 15]. Despite a higher solid loading, Y_2O_3 suspensions displayed a much lower viscosity than TiO_2 suspensions (difference of about one order of magnitude), especially at low shear rates. This huge difference is believed to arise from three different factors:

- The particles shape differences: Y_2O_3 particles platelet shape grant them the ability to align and slide easily (without much resistance) on each other when the suspension is sheared, as it was observed by several authors [15, 36, 37, 38]. The aggregated nanospheres shape of the TiO_2 particles is rough and thus induces significant friction

on each other when the suspension is sheared, hindering their movement and thus inducing shear resistance, according to Heine *et al.* [39].

- The particle size distribution: the Y_2O_3 particle size distribution is much broader than the TiO_2 particle size distribution (see Fig. 1). Lowering viscosity with broadening particle size distribution is a phenomenon already widely known and studied in the literature by authors such as Greenwood *et al.* [16] or Luckham *et al.* [40].

- The nanoparticle fraction: TiO_2 powder contains an important proportion of nanosized (< 100 nm) particles, while Y_2O_3 powder does not (see Fig. 1). Nanosized powders are known in the literature to give (at equal solid content) more viscous suspensions compared to micron-sized powders [41, 42, 43].

For both TiO_2 and Y_2O_3 powders, the results presented in Fig. 4 indicate that the optimal amount of Darvan CN dispersant is around 0.5 wt% of the dry powder to obtain the lowest suspension viscosity. This could be attributed to enhancement of the zeta potentials of the powders due to the adsorption of dispersant macromolecules on the particles surface. Such a high zeta potential induced by dispersant adsorption prevent the particles from flocculating and thus forming three dimensional particle networks in the suspension which are responsible for the suspension viscosity increase at low shear rate [37, 44]. In addition to simply prevent particle flocculation and agglomeration in the suspension, the layer of dispersant macromolecules absorbed on the particles surface also tends to facilitate particles relative movements when close to each other by reducing friction forces and thus decreasing the suspension viscosity a high shear rate, as explained by Wang *et al.* [44]. For dispersant amounts higher than 0.5 wt%, the particles surface are fully covered with absorbed dispersant, so the extra amount of dispersant remains unadsorbed (free) in the solvent, causing the suspension viscosity to increase slightly [44].

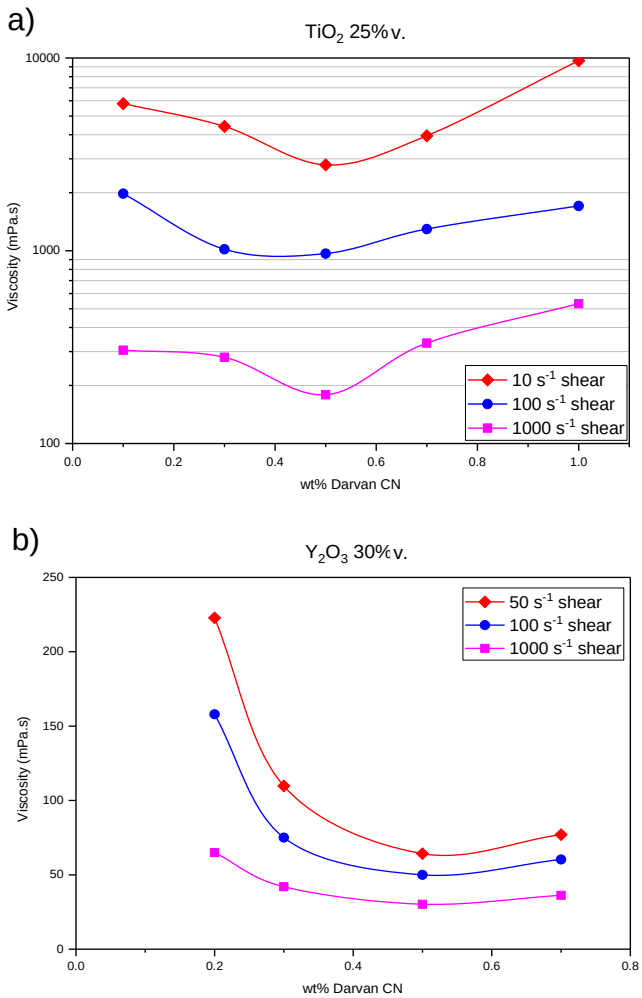

Fig. 4: Viscosity of 25 %v TiO_2 (a) and 30 %v Y_2O_3 (b) suspension vs. Darvan CN wt% at different shear rates.

3.4 Mixed TiO_2-Y_2O_3 suspensions

3.4.1 Effect of the yttrium atomic ratio

Mixed TiO_2-Y_2O_3 suspensions were prepared to assess the yttrium atomic ratio (Y/(Ti + Y)) effect on the suspension properties. Acoustophoresis revealed that the yttrium atomic percentage has a great influence on the suspension zeta potential (Fig. 5), even in small proportions (5-15 at% Y). This may be due to the Y_2O_3 particles platelet shape. Such morphology may grant the Y_2O_3 particles an hydrodynamicity different from that of the spherical particles, and/or may induce face-edge surface charge heterogeneities, as observed by several authors for various types of solid particles [36, 45, 46]. This heterogeneous charge repartition at the particles surface causes the Y_2O_3 particles to be overrepresented in the computation of the TiO_2-Y_2O_3 suspension overall zeta potential. Below pH 9, TiO_2 and Y_2O_3 particles have opposed surface charges. Thus, particle heterocoagulation [47] is highly likely to occur in this pH domain. This statement is confirmed by the fact that the overall zeta potential of TiO_2-Y_2O_3 mixed suspensions are quite close to zero below pH 9. Above pH 9, the curve overshoots between the Y_2O_3 and mixed TiO_2-Y_2O_3 (10 and 15 at% Y) suspensions are believed to be due to measurement incertitude, which could be quite high for particles with low surface charge.

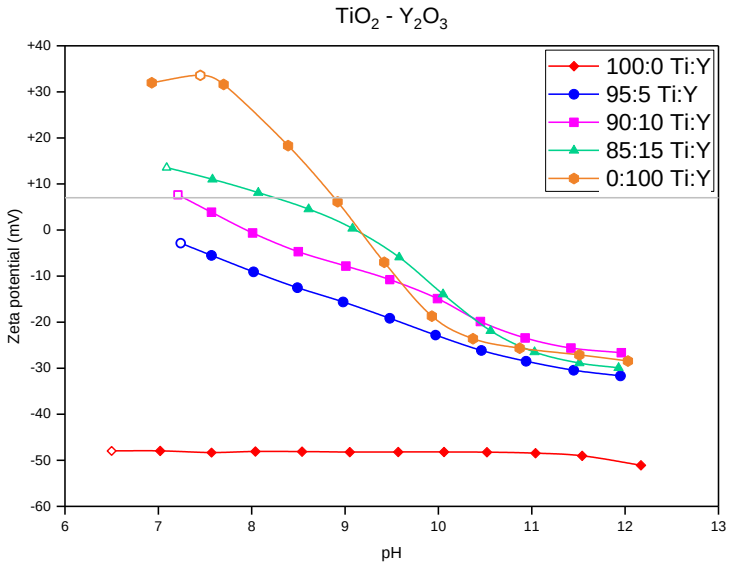

Fig. 5: Zeta potential of 1.25 %v TiO_2-Y_2O_3 suspensions of various Ti-Y atomic proportions vs. pH (hollow dots correspond to natural pH).

Sedimentation tests confirmed the role of the Y-Ti proportion on the stability of TiO_2-Y_2O_3 suspensions (see table 2 and Fig. 6). The higher the yttrium proportion, the higher the sedimentation rate. Fig. 6 also clearly indicates that the TiO_2-Y_2O_3 suspensions with 10 and 15 at% Y are significantly flocculated after 24 hrs of rest, while TiO_2-only and Y_2O_3-only suspensions remain well dispersed. This observation can be related to the suspensions zeta potentials. The ones with high zeta potentials (in absolute value) remain dispersed, while those with low zeta potentials (in absolute value) are highly flocculated. That phenomenon is caused by heterocoagulation [47] of TiO_2 and Y_2O_3 particles, i.e. flocculation induced by electrostatic attraction of these opposite-charged particles. In brief, TiO_2-Y_2O_3 suspensions (containing Y in proportions 5 to 15 at%) , when prepared without any dispersant, are low viscous when sheared but flocculate and settle quickly when laid to rest.

To dig this way further, a TiO_2-Y_2O_3 (15 at% Y) diluted suspension was observed by environmental SEM (under 700 Pa water vapor pressure, i.e. 98 % relative humidity). The resulting SEM micrographs (Fig. 7) shown a good affinity and close contact between TiO_2 nanospheres and Y_2O_3 platelets, while no Y_2O_3 particles agglomerate was noticed. These observations correlate the above statement made about the strength of the TiO_2-Y_2O_3 particles attraction from which heterocoagulation arises.

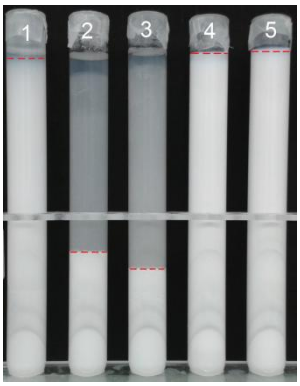

Fig. 6: Visual aspect of TiO_2-Y_2O_3 suspensions (1.25 %v solid content) with various Y proportions after 24 hrs sedimentation. Tube numbers refer to table 2.

Tube #	1	2	3	4	5
Solid composition	Y O	TiO - Y O 15 at% Y	TiO - Y O 10 at% Y	TiO - Y O 5 at% Y	TiO
Zeta potential (mV)	+ 32	+ 13	+ 8	- 3	- 48
Suspension pH	7.5	7.1	7.2	7.3	6.5

Table 2: Characteristics of TiO_2-Y_2O_3 suspensions (1.25 %v solid content) with various Y proportions after 24 hrs sedimentation, depicted in Fig. 6.

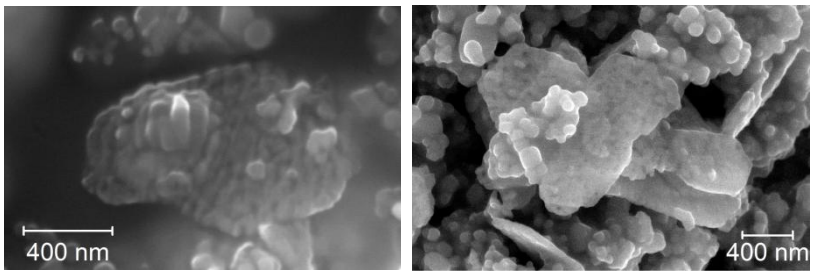

Fig. 7: Environmental SEM micrographs of a TiO_2-Y_2O_3 diluted suspension.

3.3.2 Modeling of the particle-particle interaction

Interactions between particles in suspension were modeled using the DLVO (Derjaguin, Landau, Verwey, Overbeek) particle-interaction and Hamaker theories [48, 49, 50, 56]. Interaction energy between two particles was calculated using two contributions. Equation (1) refers to the electrostatic repulsive energy. Equations in Tab. 3 refer to the attractive (van der Walls) energy contributions, for different bodies geometries. When needed, hydrodynamic forces [35] (occurring when suspension is sheared) were also taken into account with equation (2). TiO_2 particles were modeled by spheres of 100 nm diameter and Y_2O_3 particles were modeled by 1 µm square plates. Surface charges were set at – 45 and +19 mV for TiO_2 and Y_2O_3 particles respectively. The ionic strength was set at 10^{-2} mol/L in agreement with the suspension preparation protocol detailed in part 2.1.3.

$$E_{repulsion} = \frac{\varepsilon a_1 a_2 (\psi_1{}^2 + \psi_2{}^2)}{4 a_1 a_2} \left[\frac{2\psi_1 \psi_2}{\psi_1{}^2 + \psi_2{}^2} ln\left(\frac{1+e^{-\kappa D}}{1-e^{-\kappa D}}\right) + ln\left(1 - e^{-2\kappa D}\right) \right] \quad (1)$$

Bodies geometry	$E_{attraction}$
Two flat surfaces (per unit area)	$\frac{-A}{12\pi D^2}$
Sphere of diameter a near a flat surface	$\frac{-Aa}{12D}$
Two spheres of diameters a_1 and a_2	$\frac{-A}{12D}\left(\frac{a_1 a_2}{a_1 + a_2}\right)$

Table 3: Van der Walls attractive energy equations for three different bodies geometries

$$E_{hydro} = 6\pi\eta a 2\dot{\gamma} D \quad (2)$$

In the expressions above: ε is the water dielectric constant (7.09 x 10^{-10} C^2/J.m at 20°C), a is the particle diameter for a sphere/flat surface interaction, $a_{1,2}$ are the particles diameters for a sphere/sphere interaction, ψ is the particle zeta potential, κ is the inverse Debye length (calculated with equation (3), where I is the ionic strength), D is the interparticle distance, η is the solvent viscosity (1.0 mPa.s for water), $\dot{\gamma}$ is the shear rate, and A is the particle Hamaker constant. TiO_2 and Y_2O_3 Hamaker constants were set at 5.35 x10^{-20} J and 3.03 x10^{-20} J respectively, according to literature values [58]. For TiO_2-Y_2O_3 particle interaction, the approximation of equation (4) was used to obtain the global Hamaker constant of that interaction configuration.

$$\kappa\ (nm^{-1}) \approx \frac{0{,}304}{\sqrt{I(mol/L)}} \quad (3)$$

$$A \approx \sqrt{(A_1 A_2)} \quad (4)$$

The total energy is then calculated by summing the different contributions according to the different situations considered. The results of the modeling (Fig. 8) revealed that TiO_2-Y_2O_3 and TiO_2-TiO_2 interactions are far more likely to happen (lower interaction energy) than Y_2O_3-Y_2O_3 interactions. It is also to notice that suspension shear strengthens the repulsion between particles at ranges above 20 nm but the previous trend and conclusions remain the same.

These preferential particle interactions highlighted by the modeling correlate the zeta potentials measured for the TiO_2-Y_2O_3 suspensions (Fig. 5). Indeed, zeta potentials measured for TiO_2-Y_2O_3 suspensions were closer to Y_2O_3 zeta than TiO_2 zeta, in spite of Y_2O_3 being the minor component (15 at% Y). In other words, the fact that TiO_2-Y_2O_3 interactions are stronger than Y_2O_3-Y_2O_3 interactions explains why Y_2O_3 is over represented in TiO_2-Y_2O_3 suspensions zeta potentials measurements. The preferential particle interactions highlighted by the modeling are also in good agreement with the SEM observation of an heterocoagulated TiO_2-Y_2O_3 suspension (Figure 7), where a good affinity and close contact between TiO_2 nanospheres and Y_2O_3 platelets has been noticed, while no Y_2O_3 particles agglomerate was noticed.
Another particle interaction modeling was also made considering the presence of 0.5 wt% Darvan CN (an ammonium polymethacrylate dispersant, see part 3.3) in the suspension (by setting the zeta potentials at – 45 mV for both TiO_2 and Y_2O_3 particles, see part 3.3.1). The results were almost identical to those obtained in the absence of dispersant reported on Fig. 8.

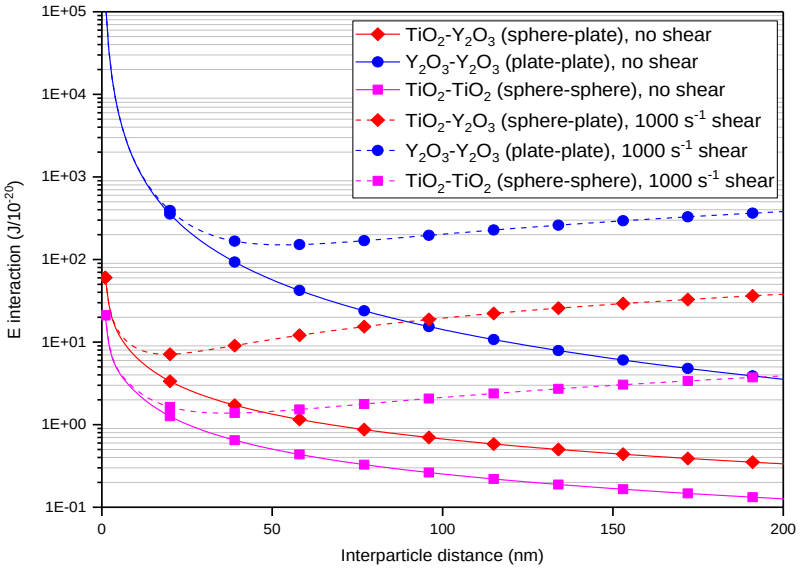

Fig. 8: Modeled interparticle interaction energy at rest (solid lines) and under 1000 s^{-1} shear (dashed lines) vs. interparticle distance.

3.3.3 Dispersion of TiO_2-Y_2O_3 mixed suspension

Optimal content of Darvan CN dispersant was assessed by acoustophoresis (Fig. 9) and sedimentation tests (Fig. 10 and Table 4) for TiO_2-Y_2O_3 (15 at% Y) suspensions.
Addition of a small amount (0.1 %) of Darvan CN to the suspension first shifted the positive zeta potential to slightly negative values. Adding more Darvan CN (0.1 - 0.3 %) makes the zeta potential more negative. A plateau region was reached (0.3 %) where addition of more dispersant does not affect the zeta potential any longer. Dispersant addition beyond this plateau (0.3 – 0.7 %) hardly alters the zeta potential. These observations were visually confirmed by sedimentation tests (Fig. 10 and Table 3). Suspensions containing 0.3 % Darvan CN or more remained dispersed after 48 hrs sedimentation, due to the highly negative zeta potential induced by Darvan CN. Suspensions with 0.1 % Darvan CN or less were not enough dispersed (low zeta potential in absolute value) and thus exhibited a highly flocculated state after 48 hrs of sedimentation.

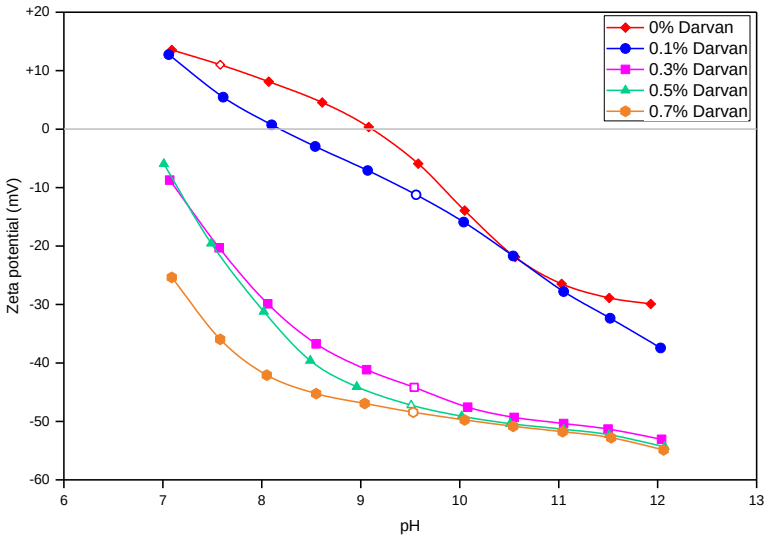

Fig. 9: Zeta potential of 1.25 %v TiO_2-Y_2O_3 (15 at% Y) suspensions vs. pH at different Darvan CN concentrations (hollow dots correspond to natural pH).

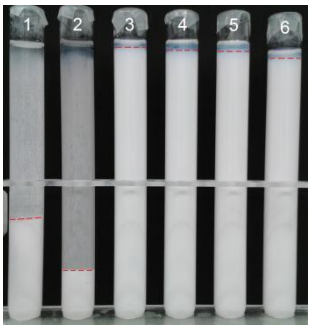

Fig. 10: Visual aspect of TiO_2-Y_2O_3 suspensions (1.25 %v solid content, 15 at% Y) with various Darvan CN contents after 48 hrs sedimentation. Tube numbers refer to table 4.

Tube #	1	2	3	4	5	6
Darvan CN content (wt % of dry powder)	0	0.1	0.3	0.5	0.75	1
Zeta potential (mV)	+ 10	- 12	- 45	- 48	- 48	- 46
Suspension pH	7.5	9.6	9.7	9.5	9.7	9.6

Table 4: Characteristics of TiO_2-Y_2O_3 suspensions (1.25 %v solid content) with various Darvan CN contents after 48 hrs sedimentation, depicted in Fig. 10.

TiO_2-Y_2O_3 suspensions of various Ti-Y proportions were prepared in the presence of 0.5 wt% Darvan CN (Fig. 11). The progressive evolution of the zeta potential profile from a TiO_2-only suspension to an Y_2O_3-only suspension can clearly be noticed, without any curve overshoot. It was not the case previously without Darvan CN (Fig. 5). This difference proves that in the presence of 0.5 wt% of Darvan CN, the heterocoagulation phenomenon does not occur any longer. Indeed, at a concentration of 0.5 wt%, the Darvan CN is able to give to all particles a surface charge negative enough to repel each other efficiently and avoid heterocoagulation.

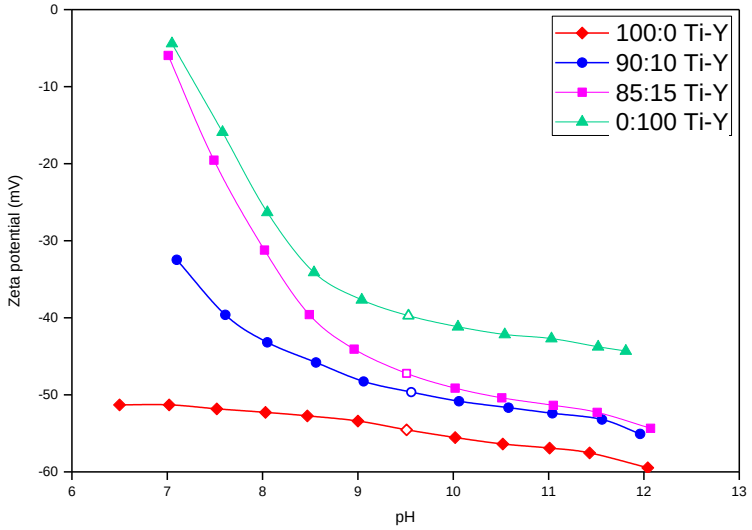

Fig. 11: Zeta potential of 1.25 %v TiO_2-Y_2O_3 suspensions of various Ti-Y atomic proportions (with 0.5 wt% Darvan CN) vs. pH (hollow dots correspond to natural pH).

The yttrium content ratio has also a great influence on TiO_2-Y_2O_3 suspension rheology (Fig. 12). Indeed, suspensions containing both TiO_2 and Y_2O_3 powders are significantly less viscous than suspensions made from the TiO_2 powder only. This synergistic effect also allowed preparation of TiO_2-Y_2O_3 (15 at% Y) suspensions with higher solid contents (up to 40 v%) than TiO_2-only or Y_2O_3-only suspensions (up to 25 and 30 v%, respectively). These solid loadings were the highest loadings achievable (with the suspensions preparation process detailed in 2.1.2) yielding suspensions that were fluid and pourable enough to be analyzed with the rheometer. Above these solid loadings, the obtained suspension was a paste that could not be easily poured and analyzed with the aforementioned rheometer.

The above mentioned phenomenon of an increase in the maximal solid loading or TiO_2-Y_2O_3 suspensions is believed to arise from two main factors. Given the TiO_2 and Y_2O_3 particle size distributions (Fig. 1), the size distribution of a 15 %at Y TiO_2-Y_2O_3 mix is broader than those of each pure powder. Thus, the small particles are able to fit in the spaces between the big particles, and so the particle packing efficiency is better. The maximum packing fraction increases (Fig. 13) for the same reason. The maximum packing fraction was calculated with the Krieger-Dougherty method [51], which is widely used in the literature to study suspensions of solid particles [40, 52, 53]. This increase of the maximum packing fraction leads to a decrease in viscosity of the suspension, as it was observed and explained by several authors [40, 52, 53]. Particle shape differences could also explain the viscosity reduction. The edge/face charge heterogeneities born by particles of certain peculiar shapes (especially platelet-shaped particles) could grant them the ability to disrupt the three dimensional networks formed by other particles by agglomeration, and thus reduce the viscosity of suspensions containing such type of objects. This phenomenon was observed for kaolinite-halloysite [54] and kaolinite-mica [55] suspensions.

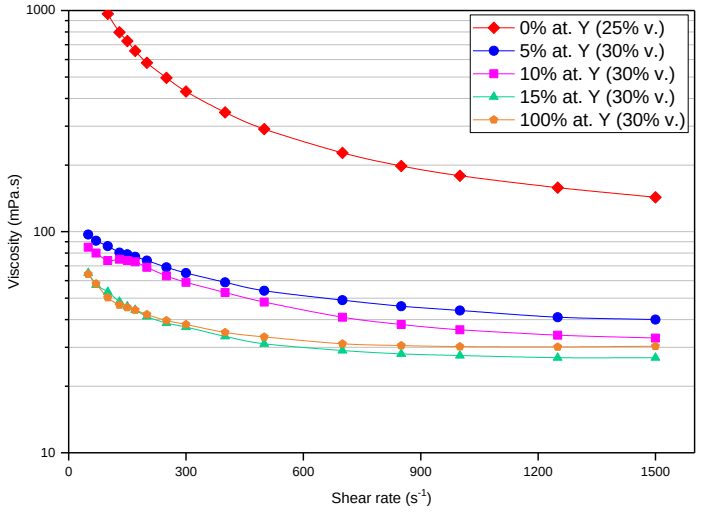

Fig. 12: Viscosity of TiO_2-Y_2O_3 suspensions with various Y proportions (with 0.5 % Darvan CN, total solid content in brackets) vs. shear rate.

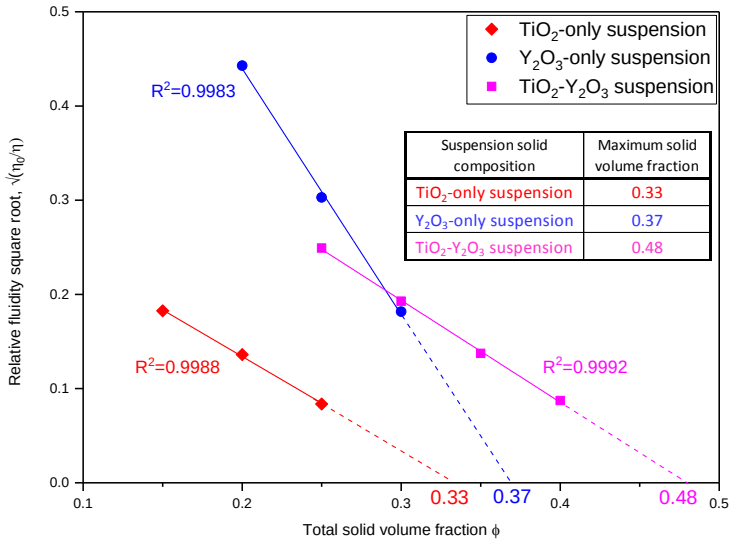

Fig. 13: TiO_2, Y_2O_3 and TiO_2-Y_2O_3 (15 at% Y) suspensions (with 0.5 wt% Darvan CN) maximal volume fractions determined by the Krieger-Dougherty plotting method.

The rheology of the TiO_2-Y_2O_3 suspension (15 at% Y) was also assessed to study the effects of Darvan CN on the viscosity (Fig. 14). It appears that the optimal concentration of this dispersant is around 0.5 wt% to have the lowest possible viscosity. This result is consistent with those obtained previously on the optimal Darvan CN concentration of the single powder suspensions (Fig. 4), also assessed at 0.5 wt% Darvan CN for both powders.

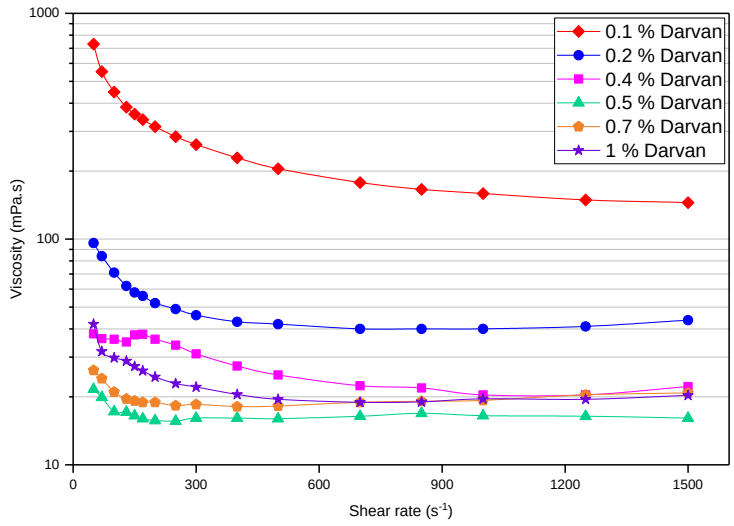

Fig. 14: Viscosity of TiO_2-Y_2O_3 suspensions (25 %v solid content, 15 at% Y) with various Darvan CN concentrations vs. shear rate.

4. Conclusion and perspectives

In this paper, high solids loading TiO_2-Y_2O_3 water-based suspensions were studied. Their elaboration process and formulation were investigated and optimized to ensure the highest fluidity and dispersion state possible, while at the same time having a high solid content. Moreover, the phenomenon of heterocoagulation between the naturally oppositely charged TiO_2 and Y_2O_3 particles has been avoided thanks to the use of an ammonium polymethacrylate dispersant (Darvan CN). In his aim, an effective suspension preparation process, involving powder deagglomeration with grinding balls, was successfully used. Moreover, optimal amounts of suitable organic dispersant (Darvan CN) were determined to ensure the best suspension processability.

Besides, a helpful phenomenon for the preparation of these suspensions was observed. Mixed together (at 5 to 15 %at Y), the TiO_2 and Y_2O_3 powders give less viscous suspensions than those made from the single powders, at equal solid contents. This

behavior is believed to arise mainly from the broadening of the particle size distribution when TiO_2 and Y_2O_3 are used together in suspension.
It has also been highlighted that surrogate powders key features like particle morphology, size distribution and surface charge have important consequences on the main suspension properties like viscosity, maximal packing fraction and settling resistance. In the present case, the key features of the TiO_2 and Y_2O_3 surrogating powders were proven to be close to the desired ones (i.e. those of UO_2 and PuO_2 powders, respectively) with the sole exception of the TiO_2 powder PZC which was surprisingly quite different from that of UO_2. However, the use of a dispersant (Darvan CN in the present case) tends to minimize this difference by giving all powders the same strong negative surface charge.
The results from this work will be used as a basis to investigate suspension shaping processes, like slip-casting or spray-freeze-drying to manufacture fuel pellets. The outcome of these investigations will be published in a future paper.

Acknowledgements

This study is supported by the *Commissariat à l'Energie Atomique* (CEA) in partnership with the Institute of Research for Ceramics (IRCER). The authors are thankful to A. Aimable and S. Blanchet from the IRCER Limoges for the technical help and advice provided during experiments. F. La Lumia thanks the PRAFA project for financial support of the Ph.D. and internship. The authors appreciate continued helpful discussions, advice, and assistance from D. W. Cannon from Colloidal Dynamics, Inc.

References

[1] D. Haas, A. Vandergheynst, J. van Vliet, R. Lorenzelli, J-L. Nigon. Mixed-Oxide Fuel Fabrication Technology and Experience at the Belgonucléaire and CFCa Plants and Further Developments for the MELOX Plant, *Nuclear Technology 106*, pp. 60-82, 1994. DOI: 10.13182/NT94-A34950

[2] J.S. Reed. Principles of ceramics processing. New York, USA. *John Wiley & Sons*, pp. 277–304, 1995

[3] V. Tsakaloudi, G. Kogias, V. Zaspalis. Freeze Granulation: A novel technique for low-loss Mn-Zn ferrites. *International Magnetics Conference 2008* (INTERMAG 2008), Madrid, Spain, 2008

[4] Q. Xu, B. Gabbitas, S. Matthews, D. Zhan. The effect of binder and plasticizer on porous titanium compacts prepared by slip casting. *Procedia Materials Science* 4, pp. 81–84, 2014.

[5] R. Greenwood. Review of the measurement of zeta potentials in concentrated aqueous suspensions using electroacoustics. *Advances in Colloid and Interface Science* 106, pp. 55–81, 2003.

[6] R. W. O'Brien, D. W. Cannon, W. N. Rowlands. Electroacoustic determination of particle size and zeta potential. *Journal of colloid and interface science* 172, pp. 406-418, 1995.

[7] J. K. Beattie, A. Djerdjev. Rapid electroacoustic method for monitoring dispersion: zeta potential titration of alumina with ammonium poly(methacrylate). *Journal of the American Ceramic Society* 83 (10), pp. 2360–64, 2000.

[8] F. F. Lange. Powder processing science and technology for increased reliability. *Journal of the American Ceramic Society* 72, pp. 3–15, 1989.

[9] L. Bergstorm, C.H. Schilling, I.A. Aksay. Consolidation behavior of flocculated alumina suspensions. *Journal of the American Ceramic Society* 75 (12), pp. 3305–14, 1992.

[10] E. Carlstrom. Surface and colloid chemistry in ceramics: an overview. In: Pugh RJ, Bergstrom L, editors. Surface and colloid chemistry in advanced ceramic processing. New York: *Marcel Dekker*, p. 1–28, 1994.

[11] W.M. Sigmund, N.S Bell, L. Bergstrom. Novel powder-processing methods for advanced ceramics. *Journal of the American Ceramic Society* 83(7), pp.1557–74, 2000.

[12] R. Greenwood, K. Kendall. Selection of suitable dispersants for aqueous suspensions of zirconia and titania powders using acoustophoresis. *Journal of the European Ceramic Society* 19, pp. 479-488, 1999.

[13] F. F. Lange. Powder processing science and technology for increased reliability. *Journal of American Ceramic Society* 72, pp. 3-15, 1989.

[14] D. J. Shaw. Introduction to Colloid and Surface Chemistry. *Butterworth Heinemann*, Oxford, 1992.

[15] S.M. Olhero, J.M.F. Ferreira. Influence of particle size distribution on rheology and particle packing of silica-based suspensions. *Powder Technology* 139, pp. 69– 75, 2004.

[16] R. Greenwood, P.F. Luckham, T. Gregory. The effect of diameter ratio and volume ratio on the viscosity of bimodal suspensions of polymer lattices. *Journal of Colloid Interface Science* 191, pp. 11 –21, 1997.

[17] R.J. Hunter. Zeta Potential in Colloid Science. *Academic Press*, New York, 1981.

[18] B. Aiken, W. P. Hsu, E. Matijevic. Preparation and properties of monodispersed colloidal particles of lanthanide compounds: III, yttrium(II1) and mixed yttrium(II1)/cerium(III) systems. *Journal of the American Ceramic Society* 71, pp. 845-853, 1988.

[19] R. Sprycha, J. Jablonski, E. Matijevic. Zeta Potential and Surface Charge of Monodispersed Colloidal Yttrium(Ill) Oxide and Basic Carbonate. *Journal of Colloid and Interfaces Science* 149, No. 2, pp. 563, 1992.

[20] Kosmulski, M., Compilation of PZC and IEP of sparingly soluble metal oxides and hydroxides from literature, *Advances in Colloid and Interface Science* 152, pp. 14-25, 2009.

[21] I. S. Bouhaik, P. Leroy, P. Ollivier, M. Azaroual, L. Mercury. Influence of surface conductivity on the apparent zeta potential of TiO2 nanoparticles: Application to the modeling of their aggregation kinetics. *Journal of Colloid and Interface Science* 406, pp. 75–85, 2013.

[22] K. Suttiponparnit, J. Jiang, M. Sahu, S. Suvachittanont, T. Charinpanitkul, P. Biswas. Role of surface area, primary particle size, and crystal phase on titanium dioxide nanoparticle dispersion properties. *Nanoscale Research Letters*, pp. 6-27, 2011.

[23] Marek Kosmulski. The significance of the difference in the point of zero charge between rutile and anatase. *Advances in Colloid and Interface Science* 99, pp. 255–264, 2002.

[24] D.L. Liao, G.S. Wub, B.Q. Liao. Zeta potential of shape-controlled TiO2 nanoparticles with surfactants. *Colloids and Surfaces A: Physicochemical Engineering Aspects* 348, pp. 270–275, 2009.

[25] L. Yezek, R.L. Rowell, M. Larwa, E. Chibowski. Changes in the zeta potential of colloidal titanium dioxide after exposure to a radio frequency electric field using a circulating sample. *Colloids Surfaces A* 141, pp. 67–72, 1998.

[26] A. Fernandez-Nieves, F.J. de las Nieves. The role of ζ potential in the colloidal stability of different TiO2/electrolyte solution interfaces. *Colloids Surfaces A* 148, pp. 231–243, 1999.

[27] N. Spanos, P.G. Koutsoukos. Calculation of Zeta Potential from Electrokinetic Measurements on Titania Plugs. *Journal of Colloidal Interface Science* 214, pp. 85–90, 1999.

[28] R. M. Cornell, A. M. Posner, J. P. Quirk. A Titrimetric and Electrophoretic Investigation of the pzc and the iep of Pigment Rutile. *Journal of Colloid and Interface Science* 53, 1975.

[29] M. Wiśniewska, K. Terpiłowski, S. Chibowski, T. Urban, V.I. Zarko, V.M. Gun'ko. Effect of polyacrylic acid (PAA) adsorption on stability of mixed alumina silica oxide suspension. *Powder Technology* 233, pp. 190–200, 2013.

[30] S. Chibowski, M. Wiśniewska, T. Urban. Influence of solution pH on stability of aluminum oxide suspension in presence of polyacrylic acid, *Adsorption* 16, pp. 321–332, 2010.

[31] M. Wisniewska, S. Chibowski, T. Urban, D Sternik. Investigation of the alumina properties with adsorbed polyvinyl alcohol. *Journal of Thermic Analysis Calorimetry* 103, pp. 329–337, 2011.

[32] S. Chibowski, M. Wisniewska, A.W. Marczewski, S. Pikus. Application of the SAXS method and viscometry for determination of the thickness of adsorbed polymer layers at the ZrO2–polymer solution interface. *Journal of Colloid and Interface Science* 267, pp. 1–8, 2003.

[33] H. G. Yang, C. Z. Li, H. C. Gu, T. N. Fang. Rheological Behavior of Titanium Dioxide Suspensions. *Journal of Colloid and Interface Science* 236, pp. 96–103, 2001

[34] L. Bergstrom. Shear thinning and shear thickening of concentrated ceramic suspensions. *Colloids Surfaces A* 133, pp. 151–155, 1998.

[35] N. Willenbacher, K. Georgieva. Product Design and Engineering: Formulation of Gels and Pastes, First Edition. *Wiley-VCH Verlag GmbH & Co*, 2013.

[36] S. Jogun, C. F. Zukoski. Rheology of dense suspensions of platelike particles. *Journal of Rheology* 40, pp. 1211, 1996.

[37] S.J. Jogun. Shear-induced structures in suspensions of anisometric colloidal particles. *M. S. thesis, University of Illinois*, 1995.

[38] N. Cruz, Y. Peng. Rheology measurements for flotation slurries with high clay contents – A critical review. *Minerals Engineering* 98, pp. 137–150, 2016.

[39] D. R. Heine, M. K. Petersen, G. S. Grest. Effect of particle shape and charge on bulk rheology of nanoparticle suspensions. *Journal of Chemical Physics*, 2010

[40] P. F. Luckham, M. A. Ukeje. Effect of particle size distribution on the rheology of dispersed systems. *Journal of Colloid and Interface Science* 220, pp. 347–356, 1999.

[41] A. A. Zaman, B. M. Moudgil. Rheology of bidisperse aqueous silica suspensions: A new scaling method for the bidisperse viscosity. *Journal of Rheology* 42, pp. 21, 1998.

[42] R. L. Hoffman. Factors affecting the viscosity of unimodal and multimodal colloidal dispersions. *Journal of Rheology* 36, pp. 947, 1992.

[43] R. F. Storms, B. V. Ramarao, R. H. Weiland. Low shear rate viscosity of bimodally dispersed suspensions. *Powder Technology* 63, pp. 247-259, 1990.

[44] X. Wang, R. Wang, C. Peng, H. Li. Rheology of aqueous BeO suspension with NH_4PAA as a dispersant. *Progress in Natural Science: Materials International* 22 (4), pp. 347–353, 2012.

[45] S. B. Johnson, A. S. Russell, P. J. Scales. Volume fraction effects in shear rheology and electroacoustic studies of concentrated alumina and kaolin suspensions. *Colloids and Surfaces A: Physicochemical and Engineering Aspects* 141, pp. 119–130, 1998.

[46] A. Nosrati, J. Addai-Mensah, W. Skinner. Rheology of aging aqueous muscovite clay dispersions. *Chemical Engineering Science* 66, pp. 119–127, 2011.

[47] L. Liang, L. Wang, A. V. Nguyen, G. Xie. Heterocoagulation of alumina and quartz studied by zeta potential distribution and particle size distribution measurements. *Powder Technology* 309, pp. 1–12, 2017.

[48] H. C. Hamaker. The London-van der Waals attraction between spherical particles. *Physica*, 4(10), pp. 1058-1072, 1937.

[49] J. N. Israelachvili, Intermolecular and Surface Forces. Academic Press, *Elsevier (NL)*, Third edition 2011, ISBN: 978-0-12-375182-9

[50] P. A. Smith, R. A. Haber. Effect of particle packing on the filtration and rheology behavior of extended size distribution alumina suspension. *Journal of the American Ceramic Society* 78 (7), pp. 1737-1744, 1995.

[51] I. M. Krieger, T. J. Dougherty. A mechanism for non-Newtonian flow in suspensions of rigid spheres. *Transactions of the Society of Rheology* 3, pp. 137, 1959.

[52] C. G. De Kruif, E. M. F. Van Iersel, A. Vrij, W. B. Russel. Hard sphere colloidal dispersions: Viscosity as a function of shear rate and volume fraction. *The Journal of Chemical Physics* 83, pp. 4717, 1985.

[53] W. Liang, T. F. Tadros, P. F. Luckham. Rheological studies on concentrated polystyrene latex sterically stabilized by poly(ethylene oxide) chains. *Journal of Colloid and Interface Science* 153. No. 1, 1992.

[54] J. Yuan, H. H. Murray. The importance of crystal morphology on the viscosity of concentrated suspensions of kaolins. *Applied Clay Science* 12, pp. 209-219, 1997.

[55] J. Merrill, L. Voisin, V. Montenegro, C. F. Ihle, A. McFarlane. Slurry rheology prediction based on hyperspectral characterization models for minerals quantification. *Minerals Engineering* 109, pp. 126–134, 2017.

[56] J. Israelachvili. (1985–2004). Intermolecular and Surface Forces. *Academic Press*. ISBN 0-12-375181-0.

[57] M. Olsson, A.-M. Jakobsson, Y. Albinsson. Surface Charge Densities of Two Actinide(IV) Oxides: UO_2 and ThO_2. *Journal of Colloid and Interface Science*, pp. 256, 256–261, 2002.

[58] L. Bergstrom. Hamaker constants of inorganic materials. *Advances in Colloidal and Interface Science* 70, pp. 125-169, 1997